ELSEVIER

Contents lists available at ScienceDirect

Science of the Total Environment

journal homepage: www.elsevier.com/locate/scitotenv



Sensitivity evaluation of the Kudryavtsev permafrost model



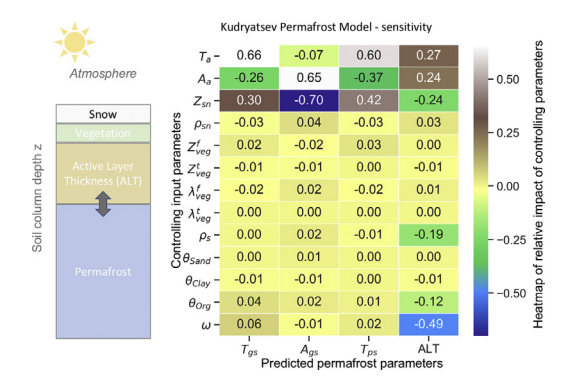
Kang Wang ^{a,b,d,*}, Elchin Jafarov ^c, Irina Overeem ^{b,d}

- ^a School of Geographic Sciences, East China Normal University, Shanghai 200241, China
- ^b CSDMS, Institute of Arctic and Alpine Research, University of Colorado Boulder, Boulder, CO 80309, USA
- ^c Earth and Environmental Sciences Division, Los Alamos National Laboratory, Los Alamos, NM 87545, USA
- ^d Department of Geological Sciences, University of Colorado Boulder, Boulder, CO 80309, USA

HIGHLIGHTS

- A reduced complexity permafrost model was evaluated to inform future users
- Permafrost temperature depends on air temperature, amplitude, and snow depth.
- Soil water bias controls uncertainty in active layer depth predictions.

GRAPHICAL ABSTRACT



ARTICLE INFO

Article history: Received 13 December 2019 Received in revised form 22 February 2020 Accepted 23 February 2020 Available online 25 February 2020

Editor: Christian Herrera

Keywords: Permafrost Thermal regime Model Alaska Soil Climate

ABSTRACT

Modeling is an important way to assess current and future permafrost spatial distribution and dynamics, especially in data poor areas like the Arctic region. Here, we evaluate a physics-based analytical model, Kudryavtsev's active layer model, which is widely used because it has relatively few data requirements. This model was recently incorporated into a component modeling toolbox, allowing for coupled modeling of permafrost and geomorphic processes over geological timescales. However, systematic quantitative assessment of the influence of its controlling parameters on permafrost temperature and active layer thickness predictions has not been undertaken before. We investigate the sensitivity of the Kudryavtsev's active layer model by Monte Carlo simulations to generate probability distributions for input parameters and compare predictions with a comprehensive benchmark dataset of in-situ permafrost observations over entire Alaska. Predicted permafrost surface temperature is highly dependent on mean annual air temperature (r = 0.78 on average), annual temperature amplitude (-0.41), and winter-averaged snow thickness (0.30). Uncertainty of predicted permafrost temperature is relatively small (RMSE = 1 °C), when air temperature and snow depth are well constrained. Similarly, RMSE between simulated and observed ALT at stations is ~0.08 m. However, under given air temperature and snow conditions, soil water content bias can significantly affect modeled active layer thickness (RMSE = 0.1 m or 40% of the observed active layer thickness). If soil water content has a large bias, improvements in other parameters may not significantly improve the active layer predictions of the Kudryavtsev's model.

© 2020 Elsevier B.V. All rights reserved.

^{*} Corresponding author at: School of Geographic Sciences, East China Normal University, Shanghai 200241, China. E-mail address: kwang@geo.ecnu.edu.cn (K. Wang).

1. Introduction

Permafrost-affected soils occupy a large portion of land in the Northern Hemisphere (Zhang et al., 1999). Warming of permafrost-affected soils imposes direct impacts on to the Arctic ecosystems and damages infrastructure build on permafrost (Melvin et al., 2017). Even more importantly, warming permafrost has a potential for significant positive global climate feedback due to carbon and methane emissions from decomposition of large stocks of previously frozen organic material (Schuur et al., 2015; MacDougall, 2016; McGuire et al., 2016; McGuire et al., 2018; Moon et al., 2019). The deepening of the 'active layer', the maximum seasonal thawed depth (i.e., active layer thickness) to which the permafrost thaws every year, drives such emissions. Modeling of permafrost thermal dynamics at different spatial scales requires integrating site-specific observations and best available data as regional or even global scale maps. There are many different models to simulate historical or predict future permafrost dynamics, using different parameterization and algorithms, although the representation of the thermal physical processes are rather similar (Goodrich, 1982; Zhang et al., 1996; Ling and Zhang, 2004; Marchenko et al., 2008; Jafarov et al., 2012; Westermann et al., 2013). Disentangling the complex interactions of different environmental factors on permafrost thermal dynamics is an essential step in identifying gaps in the required input data and in assessing suitability of the model for predictive purposes.

Sensitivity analysis is one important approach to better understand the complex interaction between different environmental factors contributing to changes in the subsurface temperatures and active layer thickness predictions. Sensitivity analysis requires a large number of models runs with different combinations of input variables and parameters. For numerical models that have a vast number of parameters it becomes difficult to include all systematically in sensitivity analysis and appropriately benchmark. Then again, initial conditions and time-dependent boundary conditions also influence simulation results. Therefore, rigorous sensitivity analysis is more feasible for a model that is time efficient, but still captures most of the required physical processes.

Kudryavtsev et al. (1977) developed an analytical model for soil thermal state that accounts for major controls from air temperature, vegetation, snow and soil properties. In this paper, we refer to our model as "Ku model", acknowledging its original developer. Ku model provides an approximate solution of the Stefan problem (Lunardini, 1981), the classic description of a temperature distribution in a homogeneous medium undergoing a phase change. In our case, soil transitions from frozen state to thawed state on an annual basis. The Ku Model has been applied on a variety of scales, from local soil profiles to regional and global scales. Anisimov et al. (1997) used this model to explore responses of active layer thickness under different climate scenarios across the Northern Hemisphere. Shiklomanov and Nelson (1999) calculated the active layer thickness in the Kuparuk River Basin in Alaska. Sazonova and Romanovsky (2003) further developed the model to calculate the thermal state in Alaska and East Siberian transects at 0.5-degree resolution. Streletskiy et al. (2012) used the model to investigate the spatial variability of active layer thickness in northern Alaska also at 0.5-degree resolution. Panda et al. (2016) calculated permafrost distribution at ~30 m resolution in National Parks in Alaska. However, each of these applications imposed expert-informed unique suites of parameters for each type of landscape. And, whereas these studies showed good agreements with in-situ active layer thickness observations, we argue the permafrost community benefits from a more rigorous study of each of the parametrizations in this model. Ku model results match closely with numerical model results, such as the Goodrich model (Goodrich, 1982; Romanovsky and Osterkamp, 1997) and land surface models (Sazonova and Romanovsky, 2003), because of similarity in the modeled physical processes. Thus, identifying which parameters control most significantly predictions of the Ku model, would also be indicative for the sensitivity to environmental input parameters of more complex numerical models.

An additional reason to evaluate the Ku model is its implementation as a component in the Permafrost Modeling Toolbox (Overeem et al., 2018). This toolbox of coupled permafrost and earth-surface process models is designed to be flexible to allow combined modeling of thermal processes and geomorphological and sedimentary system feedbacks. Ku model is one component, with both simpler and more complex permafrost process models also being available within the toolbox (https://github.com/permamodel). To simulate geomorphic and permafrost processes over longer timescales, like full glacial-interglacial cycles of 10s to 100s of thousands of years, a computationally efficient and intermediate complexity model with relatively modest data requirements is imperative. Any future coupled experiments can be undertaken more informed when a rigorous sensitivity analysis of the Ku model is undertaken.

Our overarching goal is to quantify Ku model outputs using sensitivity analysis to better understand the effect of vegetation, snow and soil texture on ground temperature regime and active layer thickness (ALT). Here we assess how important environmental factors affect model output and what improvements in existing data products would improve regional to global modeling of permafrost. To validate model results we use observed ground temperature from Global Terrestrial Network for Permafrost (GTN-P) (Biskaborn et al., 2015) and ALT from Circumpolar Active Layer Monitoring (CALM) observations (Brown et al., 2000; Burgess et al., 2000; Shiklomanov et al., 2008) across Alaska. Finally, we evaluate the uncertainties of permafrost simulations by using high-resolution monthly climate datasets (2 km) from Scenarios Network for Alaska and Arctic Planning (SNAP) over Alaska. In this way, we aim to thoroughly document the Ku model component and its capabilities for future users within the context of the permafrost toolbox.

2. Methods

2.1. Overview of the study area

Our study area covers most of Alaska (Fig. 1), comprising a large geographical extent (59–71°N, 139–169°W), complex topography, climate, and a variety of landscapes. Mean annual air temperature ranges roughly from -11 to 8 °C and the observed annual cumulative precipitation ranges from 100 to 6000 mm. We here report 30-year 'climate normals' over 1981–2010, available at http://akclimate.org/Climate/ Normals. Note that climate conditions and dynamics vary considerably among climate divisions (Bieniek et al., 2012; Bieniek et al., 2014). Land cover types in our study area are mainly tundra, meadows, and boreal forest (Nowacki et al., 2001). More than 80% of this area is underlaid by permafrost (Jorgenson et al., 2008). Continuous, discontinuous, sporadic, and isolated permafrost each occupy approximately 32%, 31%, 8%, and 10% of Alaska, respectively (Jorgenson et al., 2008). Borehole temperature measurements show that the permafrost base is generally 200–660 m below ground surface in the region north of the Brooks Range (Jorgenson et al., 2008). In contrast, the southwest part of Alaska features isolated permafrost and the permafrost base can be limited to only several meters (Shiklomanov et al., 2008). In-situ measurements shows that active layer thickness is generally less than half meter deep north of the Brooks Range and more typically is >1.5 m in interior Alaska (Shiklomanov et al., 2008). Large organic carbon content in the active layer and permafrost (Tarnocai et al., 2009; Hugelius et al., 2013) is now considered as a crucial factor to trigger a positive climate feedback (Koven et al., 2011). We compiled a large dataset of 72 stations with soil thermal observations from the USGS climate network, the National Park Service and the University of Alaska, specifically the CALM and GTN-P networks, which is crucial in model sensitivity testing and validation for this entire region (Wang et al., 2018).

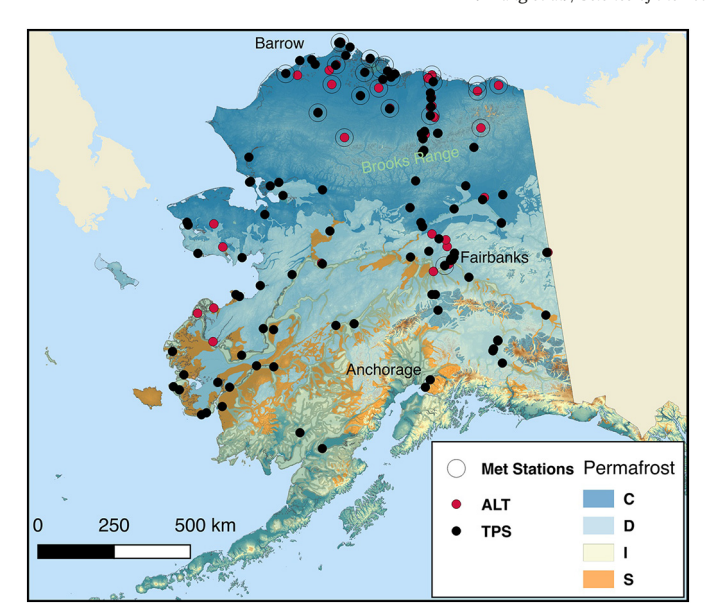


Fig. 1. Site map of active layer thickness observation locations from CALM network and ground temperature (>2 m depth) from GTN-P database. The permafrost map is modified after Jorgenson et al. (2008) (C: continuous, D: discontinuous, I: Isolated, S: sporadic permafrost). Background colors show the color shaded relief with 200-meter resolution, obtained from https://www.sciencebase.gov/catalog/item/4f4e4a85e4b07f02db64d5cb.

2.2. Model design as a component in permamodel

The Ku model is designed as a part of the permafrost modeling toolbox (permamodel). This means the model is developed under the framework of Python Modeling Toolkit (PyMT) and uses a Basic Model Interface (BMI) (Peckham et al., 2013). PyMT is an open source Python package, developed by the Community Surface Dynamics Modeling System (CSDMS). PyMT provides the functionality to couple models that expose a Basic Model Interface (BMI). BMI is a wrapped interface to facilitate communications among models. By design, the BMI is straightforward to implement in several programming languages (i.e., C, C++, Fortran, Java, and Python). The Ku model has two versions; Ku-FLEX is a version that comprises no parameterization, and offers the full suite of parameters to control. The other version, Ku model, combines the model with soil thermal parameterization data, which will be described in Section 2.3.

2.3. Theoretical description of Kudryavtsev's (Ku) model

Ku model uses an approximate analytical solution to the Stefan freeze-thaw problem, to calculate for a given vertical profile the maximum annual thawing depth and mean annual permafrost temperature (T_{ps}) at bottom of the thaw layer at steady state (Kudryavtsev et al., 1977; Anisimov et al., 1997; Romanovsky and Osterkamp, 1997; Sazonova and Romanovsky, 2003).

The schematic representation of the Ku model is shown in Fig. 2. The model contains four components; the snow insulation, vegetation effect, permafrost temperature, and thaw depth modules. Each layer shown in Fig. 2 reduces the initial air temperature amplitude and is propagated to the solution of the Stefan problem.

Ku model uses monthly mean air temperature, snow depth, and snow density as climate forcing variables and requires set parametrized vegetation coefficients, soil moisture, and soil thermal properties for each location. The nomenclature of the variables used in this formula and following after this formula can be found in Table 1.

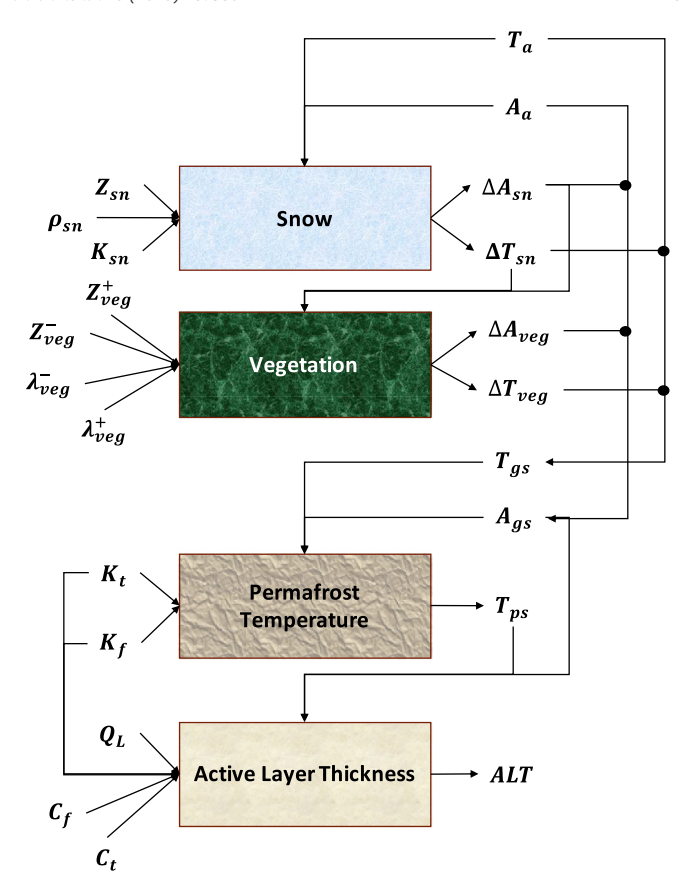


Fig. 2. Conceptual diagram for the Kudryavtsev model and schematic profile of mean annual temperature through the lower atmosphere, snow, vegetation and active layer and top of permafrost. Variable names are listed in Table 1.

2.3.1. Snow module

Snow cover reduces air temperature amplitude by ΔA_{sn} which is proportional to the change in mean annual temperature ΔT_{sn} . The empirical equation has the following form (Kudryavtsev et al., 1977):

$$\Delta T_{sn} = \Delta A_{sn} = A_a \left\{ 1 - e^{-Z_{sn} \sqrt{\left(\frac{\pi}{P \lambda_{sn}}\right)}} \right\}$$
 (1)

and $\lambda_{sn} = \frac{K_{sn}}{C_{sn}} \rho_{sn}$ is thermal diffusivity of seasonal snow cover. C_{sn} is specific heat capacity of snow (2090 J kg⁻¹ °C⁻¹). K_{sn} is snow thermal conductivity. ρ_{sn} is snow density (kg m⁻³). A_a is the annual amplitude of air temperature, i.e. half of the temperature difference between the hottest and coldest months. The ideal approach for finer time scale (e.g., daily) is to fit the annual cycle curve then make estimate of the maximum and minimum temperature.

2.3.2. Vegetation effect module

Whereas vegetation could reduce radiation absorption and interact with atmosphere, here we only consider vegetation layer as a conductive heat buffer layer. The thermal diffusivities in summer and winter time could be different in order to depict different role of vegetation on the ground. In summer time, vegetation mainly reduces heat transfer from atmosphere to the ground while in winter time will be keep heat in the ground. Thermal effect of vegetation is calculated according to (Ershov, 1971):

$$\frac{\Delta A_{\text{veg}} = \Delta A_{-} \tau_{-} + \Delta A_{+} \tau_{+}}{P} \tag{2}$$

Table 1Nomenclature used in the mathematical description of the Ku model.

Variable	Description	Unit	Range	Constraint	Reference
A_a	Air temperature amplitude	°C	[5, 30]	=	
T_a	Mean annual air temperature	°C	[-28,5]	_	
Z_{sn}	Winter-averaged snow thickness	m	[0.05, 1.50]	_	Sturm et al. (1995)
K_{sn}	Snow thermal conductivity	$W m^{-1}C^{-1}$	[0.08, 0.25]	_	Sturm et al. (1995)
ρ_{sn}	Snow density	${ m kg}~{ m m}^{-3}$	[200, 350]	_	Sturm et al. (1995)
C_{sn}	Specific heat capacity of snow	$\mathrm{J}\;\mathrm{kg^{-1}\;^{\circ}C^{-1}}$	2090	_	Anisimov et al. (1997)
Z_{veg}^f, Z_{veg}^t	Height of the vegetation for the cold and warm seasons	m	[0.0, 0.15]	$Z_{veg}^- \le Z_{veg}^+$	Anisimov et al. (1997)
$\lambda_{veg}^f, \lambda_{veg}^t$	Thermal diffusivity of vegetation in frozen and thawed state	$m^2 s^{-1}$	$[5.6 \times 10^{-8}, 1.5 \times 10^{-6}]$	$Z_{veg}^- \le Z_{veg}^+$ $\lambda_{veg}^- \ge \lambda_{veg}^+$	Anisimov et al. (1997)
K_f, K_t	Soil thermal conductivity of frozen and thawed state	$W m^{-1}C^{-1}$	[0.80, 2.65]	$K_f > K_t$	Anisimov et al. (1997)
			[0.35, 2.15]		
C_f , C_t	Volumetric heat capacity of frozen and thawed states	${\rm J} \; {\rm m}^{-3} \; {\rm ^{\circ}C^{-1}}$	$[1 \times 10^5, 8 \times 10^5]$	$C_f < C_t$	Anisimov et al. (1997)
Q_L	Volumetric latent heat of ice-water fusion	$J m^{-3}$	$[5 \times 10^7, 12 \times 10^7]$	_	
θ_{Sand} , θ_{Silt} , θ_{Clay}	Weight fraction of sand, silt, and clay in a mixed soil	_	[0, 1]	$\theta_{Sand} + \theta_{Silt} + \theta_{Clav} = 1$	
θ_{Org}	Weight fraction soil organic matter	_	[0, 1]	_	
$\rho_{\rm s}$	Soil bulk density	${\rm kg}~{\rm m}^{-3}$	[150, 1800]	_	
ω	Volumetric water content	m^3/m^3	[0.05, 0.80]	_	
λ_{sn}	Thermal diffusivity of snow	$m^2 s^{-1}$	=	_	
ΔA_{sn}	Damping of annual temperature amplitude due to snow	°C	_	_	
ΔT_{sn}	Damping of annual mean temperature due to snow	°C	_	_	
ΔA_{veg}	Damping of annual temperature amplitude due to vegetation	°C	_	_	
ΔT_{veg}	Damping of annual mean temperature due to vegetation	°C	_	_	
T_{gs}	Mean annual ground surface temperature	°C	_	_	
A_{gs}	Ground surface temperature amplitude	°C	_	_	
T_{ps}	Temperature at permafrost surface	°C	_	-	
ALT	Active layer thickness, maximum depth of seasonal thawing	m	_	_	

$$\frac{\Delta T_{\text{veg}} = \Delta A_{-} \tau_{-} - \Delta A_{+} \tau_{+}}{P} \times \frac{2}{\pi}$$
(3)

Changes in the average temperature amplitudes at the surface below and above the vegetation layer during the cold and warm seasons, called ΔA_- and ΔA_+ , are described as follows:

$$\Delta A_{-} = (A_{a} - \Delta A_{sn} - T_{a} - \Delta T_{sn}) \left\{ 1 - e^{-Z_{\text{veg}}^{-}} \sqrt{\left(\frac{\pi}{2\tau - \lambda_{\text{veg}}^{-}}\right)} \right\}$$

$$(4)$$

$$\Delta A_{+} = (A_{a} - \Delta A_{sn} + T_{a} + \Delta T_{sn}) \left\{ 1 - e^{-Z_{veg}^{+}} \sqrt{\left(\frac{\pi}{2\tau_{+}\lambda_{veg}^{+}}\right)} \right\}$$
 (5)

where T_a is mean annual air temperature. Durations of the cold $(\tau_-, \text{unit: second})$ and warm seasons $(\tau_+, \text{unit: second})$ are:

$$\tau_{-} = 86400 \times 365 \times \left(0.5 - \frac{1}{\pi} \arcsin\left(\frac{T_a + \Delta T_{sn}}{A_a} - \Delta A_{sn}\right)\right)$$
 (6)

$$\tau_{+} = 86400 \times 365 - \tau_{-} \tag{7}$$

These equations imply that vegetation can have either cooling or warming effects on the ground below.

2.3.3. Permafrost surface temperature module

Knowing air temperature and respective temperature amplitude damping within the snow cover and vegetation layers, we can calculate the annual temperature amplitude ($A_{\rm gs}$) and mean annual temperature at the ground surface below vegetation and snow ($T_{\rm gs}$):

$$T_{gs} = T_a + \Delta T_{sn} + \Delta T_{veg} \tag{8}$$

$$A_{gs} = A_a - \Delta A_{sn} - \Delta A_{veg} \tag{9}$$

To calculate ALT, we need the temperature at the top of permafrost (T_{ps}) . In some previous studies, T_{ps} was an input, derived from in-situ borehole measurements (Romanovsky and Osterkamp, 1997). However, in our implementation we use an approximation for T_{ps} (Kudryavtsev et al., 1977)

$$T_{ps} = \frac{\frac{1}{2}T_{gs}(K_f + K_t) + A_{gs}\frac{K_t - K_f}{\pi} \begin{bmatrix} T_{gs} \\ A_{gs} \end{bmatrix} arcsin(\frac{T_{gs}}{A_{gs}}) + \sqrt{1 - \frac{T_{gs}^2}{A_{gs}^2}} \\ K^*$$
 (10)

If the numerator in Eq. (10) is below zero, K^* equals K_f , i.e. thermal conductivity in frozen state, indicating permafrost. If the numerator is above zero, K^* equals K_f , i.e. thermal conductivity in thawed state, thus simulating seasonally frozen ground.

2.3.4. Active layer thickness module

Finally, the maximum depth of seasonal thawing or active layer thickness (ALT in m) has the following form:

$$ALT = \frac{2(A_{gs} - T_{ps})\sqrt{\frac{KPC}{\pi}} + \frac{(2A_{ps}CZ_c + Q_LZ_c)Q_L\sqrt{\frac{PK}{\pi C}}}{2A_{gs}CZ_c + Q_LZ_c + (2A_{ps}C + Q_L)\sqrt{\frac{PK}{\pi C}}}}{2A_{ps}C + Q_L}}$$
(11)

where $Q_L = 335200 \times \omega \times \rho_s$ wherein ω is volumetric water content, and ρ_s is soil bulk density (kg m⁻³). $[C, K] = \{ [C_f, K_f], \text{ if } T_{ps} < 0 \ [C_t, K_t], \text{ if } T_{ps} > 0. \}$

Mean annual temperature amplitude at the top of the permafrost table (A_{ps}) and Z_c (an intermediate variable used to calculate ALT) are:

$$A_{ps} = \frac{A_{gs} - |T_{gs}|}{\ln\left(\frac{A_{gs} + \frac{Q_L}{2C}}{|T_{gs}| + \frac{Q_L}{2C}}\right)} - \frac{Q_L}{2C}$$
(12)

$$Z_{c} = \frac{2(A_{gs} - |T_{gs}|)\sqrt{\frac{KPC}{\pi}}}{2A_{ps}C + Q_{L}}$$
 (13)

2.4. Snow and soil thermal parameterizations

Snow thermal conductivity (K_{sn}) is set based on snow density following Kudryavtsev et al. (1977):

$$K_{sn} = 0.7908(0.001\rho_{sn})^2$$
 (14)

To implement the Ku model, thermal parameters of soils have to be set. However, they are not measured directly and only sparsely available. More commonly available soil properties are soil texture, bulk density, and water content. Therefore, these soil data are used to estimate thermal parameters of soil (K_t , K_b , C_b , C_b).

Thermal conductivity of the mineral portion of a dry soil is estimated:

$$K_{mineral} = K_{Sand}^{\theta_{Sand}} K_{Silt}^{\theta_{Silt}} K_{Clay}^{\theta_{Clay}}$$
(15)

where $\theta_{Sand} + \theta_{Silt} + \theta_{Clay} = 1$. Typical thermal conductivities of sand, silt, and clay are from (Anisimov et al., 1997) (see also Table 2).

A top peat layer plays an important role in the permafrost thermal dynamics (Jafarov and Schaefer, 2016). Anisimov et al. (1997) considered peat soils only for cases in which the whole soil column consists of peat. Streletskiy et al. (2012) applied a simple way to include a peat layer even when peat moisture and thickness is unknown. However, detailed maps or databases of peat layer thickness over large regions are not currently available. Thus, here we consider peat through specifying the thermal conductivity of the organic matter fraction within the mineral soil:

$$K_s = K_{mineral}^{\left(1 - \theta_{\rm Org}\right)} K_{Peat}^{\theta_{\rm Org}} \tag{16}$$

Thus, the thermal conductivity of soil in frozen (K_f) and thawed (K_t) states are estimated:

$$\begin{cases} K_t = K_s^{(1-\omega)} 0.54^{\omega} \\ K_f = K_s^{(1-\omega)} 2.35^{\omega} \end{cases}$$
 (17)

Specific heat capacity of the mineral portion in a dry soil ($c_{mineral}$) is determined:

$$c_{mineral} = c_{Sand}\theta_{Sand} + c_{Silt}\theta_{Silt} + c_{Clav}\theta_{Clav}$$
(18)

Wherein typical specific heat capacities (c_{Sand} , c_{Silt} , and c_{Clay}) are again from Anisimov et al. (1997) (Table 2). For those cases with peat or high organic matter, the specific heat capacity of dry soil (c_s) is:

$$c_{\rm s} = (1 - \theta_{\rm Org}) c_{\rm mineral} + \theta_{\rm Org} c_{\rm Peat} \tag{19}$$

Table 2 Typical thermal parameters of soils.

Description	Sand	Silt	Clay	Peat
Heat capacity (J kg ⁻¹ °C ⁻¹)	690	730	900	200
Thermal conductivity of dry soil (thawed/frozen) (W m ⁻¹ °C ⁻¹)	1.05/1.25	1.05/1.25	0.90/1.15	0.35/0.80

Volumetric heat capacities of soil in frozen (C_f) and thawed (C_t) states then are:

$$\begin{cases} C_t = c_s \rho_s + 4190 \times \omega \times \rho_{water} / \rho_s \\ C_f = c_s \rho_s + 2025 \times \omega \times \rho_{water} / \rho_s \end{cases}$$
 (20)

where ρ_s is soil bulk density (kg m⁻³).

In summary, the required soil parameters include bulk density, sand fraction, silt fraction, clay fraction, organic content, and water content. Each of these parameters can be obtained from SoilGrid-1km, a recently compiled high-resolution global soil database (Hengl et al., 2014). This database presents seven layers from 0 through 2 m below the ground surface worldwide. In our approach the layers are averaged to a single soil column and then resampled to the SNAP climate data grid resolution (i.e., 2 km).

2.5. In-situ site-specific and regional comparison data

Permafrost metrics include (i) ALT and (ii) mean annual permafrost surface temperature (T_{ps}) . ALT observations are obtained from the CALM database, which comprises data collected since 1990. The active layer thickness is measured by physical probing on grids ranging in size of 100×100 to 1000×1000 m, at a single point, along transects, or from permanently installed frost tubes (Brown et al., 2000; Shiklomanov et al., 2008; Shiklomanov et al., 2016). Ground temperature data are obtained from the GTN-P network (Burgess et al., 2000). Ground temperatures are typically measured in boreholes and are often collected at depths below the permafrost surface. However, derived mean annual ground temperature has been shown to be accurate to <1 °C for observations at depths up to 40 m under a typical geothermal gradient (Westermann et al., 2015). Thus, we occasionally use deeper observations to approximate T_{ps} and verify our simulations over Alaska. In total, 53 ALT sites and 117 T_{ps} sites are used for comparisons (Fig. 1).

In-situ climate forcing data are obtained from meteorological station data compiled by Wang et al. (2018), including air temperature, snow depth, and volumetric water content. The direct inputs are listed in Table 3, which are averaged over their available time period in order to represent a steady-state climate normal. The raw dataset has 72 stations and detailed description can be found in Wang et al. (2018). We selected 21 stations to evaluate and implement sensitivity analysis, of which 10 stations have comprehensive climate measurements, as well as ALT, and T_{ps} data. There are 19 stations that have both climate observations and available ALT measurements. Available T_{ps} measurements (12 sites) from the GTN-P are listed in Table 3 for comparison. The climate parameter inputs, and ALT, and T_{ps} measurements are listed in Table 3. None of the meteorological stations feature measurements of snow water equivalent or snow density. Snow density is set to a constant of 220 kg m $^{-3}$ (Zhong et al., 2014).

Vegetation height and thermal diffusion information are rare and difficult to obtain for either cold or warm seasons. Generally, in drier tundra environments the height of vegetation does not exceed 0.10 m, and in wet tundra and moist acidic areas, it does not exceed 0.15 cm (Shiklomanov and Nelson, 1999). Therefore, vegetation height in cold and thaw seasons (Z_{veg}^- and Z_{veg}^+) are assumed to be 0.05 and 0.15 m respectively following Anisimov et al. (1997) and Shiklomanov and Nelson (1999). λ_{veg}^- and λ_{veg}^+ are 1.39 × 10⁻⁶ and 5.56 × 10⁻⁸ m² s⁻¹ following Anisimov et al. (1997).

We use SNAP monthly air temperature and precipitation at a spatial resolution of 2 km to simulate permafrost thermal dynamics across Alaska. These SNAP products are downscaled from the Climatic Research Unit (CRU) TS 4.0 dataset (1901–2015) (Walsh et al., 2018). The downscaling method accounts for the effect of topography on the near surface temperatures. SNAP products are available at the SNAP website (http://ckan.snap.uaf.edu/dataset) and details can be found in

Table 3 Comparison dataset of in-situ climate inputs and measured ALT and $T_{\rm DS}$ from 21 sites across Alaska.

Name	Lat	Lon	Onset	Final	T_a	A_a	Z_{sn}	ω	ALT	T_{ps}
	°N	°E	Year	Year	°C	°C	m	$m^{3}m^{-3}$	cm	°C
Awuna2	69.16	-158.03	2003	2015	-9.66	19.01	0.34	0.47	35	-4.1
Camden Bay	69.97	-144.77	2003	2015	-10.31	16.41	0.20	0.37	45	
Drew Point	70.86	-153.91	1998	2015	-10.71	15.86	0.20	0.39	39	-9.4
East Teshekpuk	70.57	-152.97	2004	2015	-10.14	16.80	0.23	0.45	31	
Fish Creek	70.34	-152.05	1998	2015	-10.56	17.86	0.19	0.45	30	-6.6
Ikpikpuk	70.44	-154.37	2005	2015	-10.19	18.24	0.24	0.38		-7.0
Inigok	69.99	-153.09	1998	2015	-10.44	18.91	0.22	0.37	43	-5.6
Koluktak	69.75	-154.62	1999	2015	-10.08	19.52	0.20	0.2	118	
Marsh Creek	69.78	-144.79	2001	2015	-8.54	16.37	0.19	0.41	50	
Niguanak	69.89	-142.98	2000	2015	-9.87	16.82	0.15	0.41	48	
Piksiksak	70.04	-157.08	2004	2015	-9.82	18.73	0.12	0.37	49	
Red Sheep Creek	68.68	-144.84	2004	2015	-6.86	17.46	0.25	0.35	66	
South Meade	70.63	-156.84	2003	2015	-10.35	18.20	0.20	0.45	41	
Tunalik	70.20	-161.08	1998	2015	-10.01	17.72	0.16	0.41	53	-7.1
Umiat	69.40	-152.14	1998	2015	-9.62	18.36	0.31	0.33	36	-4.8
Barrow 2	71.31	-156.66	2002	2016	-10.03	14.29	0.11	0.45	35	-9.1
Boza Creek 1	64.71	-148.29	2009	2016	-2.91	18.86	0.17	0.39		-1.2
Happy Valley	69.16	-148.84	2001	2016	-9.44	18.98	0.31	0.38	41	-5.2
Ivotuk 4	68.48	-155.74	1998	2016	-9.44	18.16	0.43	0.45	53	
West Dock	70.37	-148.55	2001	2016	-10.54	16.35	0.05	0.42	32	-10.0
Deadhorse	70.16	-148.47	1990	1998	-11.05	18.59	0.09	0.48	60	-8.4

Hijmans et al. (2005). To eliminate inter-annual variability and provide a steady-state climate normal, monthly air temperature over 1996–2015 is averaged by each month. Although there was a slightly positive trend in air temperature during this period, the inter-annual fluctuation is much more pronounced than the trend.

Snow depth and snow density inputs to the model are simulated by a snow model, originally developed by Brown et al. (2003). This model considers snow accumulation processes and requires only air temperature and precipitation as climate inputs. Additional invariant parameters are a snow classification map (Sturm et al., 1995) and a binary (forest or not) land cover map (Tuanmu and Jetz, 2014). The snow model has been validated extensively by ground-based data and provides a good estimate (Brown et al., 2003). We also compare our insitu data in Table 3 with the snow model outputs, but we note that a comprehensive uncertainty quantification of this snow model exceeds the scope of this paper. A recent study already showed that the bias of snow simulation is sourced predominantly from inconsistencies in precipitation (Brown et al., 2018). The simple snow model has been also developed under the framework of BMI and PyMT, which enable us to couple it with Ku model. The model is available at https://github.com/ permamodel/Snow_BMI_Fortran.

2.6. Parameter sensitivity study

Sensitivity analyses were implemented using the Model Analysis ToolKit (MATK) Python package (URL: http://dharp.github.io/matk/). Note that, some constraints among parameters were applied thus might reduce the total of samples (Table 1).

Firstly, we investigated the sensitivity of the parameters and inputs for the Ku model without parameterization, which is described in Eqs. (1)–(13). The Ku model outputs depend on 14 variables and parameters: T_a , A_a , Z_{sn} , ρ_{sn} , K_{sn} , Z_{veg}^+ , Z_{veg}^- , λ_{veg}^+ , λ_{veg}^- , K_t , K_f , C_t , C_f , and Q_L . In more process detail (i) snow damping effect depends on T_a , A_a , Z_{sn} , ρ_{sn} , and K_{sn} . (ii) The vegetation damping effect depends on $T_a + \Delta T_{sn}$, $A_a - \Delta A_{sn}$, Z_{veg}^+ , Z_{veg}^- , λ_{veg}^+ , and λ_{veg}^- (iii) Permafrost temperature depends on T_{gs} , A_{gs} , K_t , and K_f . (iv) Active layer thickness depends on T_{ps} , A_{gs} , K_t , K_f , C_t , C_f , and Q_L .

We used typical parameterization approaches for snow and soil properties (see Section 2.3). Therefore, a larger set of sensitivity test investigated the effects of soil and snow properties inputs directly, instead of using empirical equations (Section 2.3). In our experiments, we assume all variables and parameters are uniformly distributed in order

to analyze the model response to any possible combination of variables and parameters. Although parameter sampling is based on probability distributions, unrealistic parameter combinations are excluded from the final analysis. For example, $\theta_{Sand} + \theta_{Silt} + \theta_{Clay}$ has to equal one, while Monte Carlo sampling of these three parameters would not necessarily ensure all combinations fulfill this constraint. Thus, we removed any parameter combinations that exceed physical boundaries. Constraints and ranges of parameters are listed in Table 1.

Secondly, we evaluate uncertainty specifically for simulations of permafrost over Alaska. Using the same MATK, we test variables and parameters from measured climate forcing, air temperature, snow depth, and volumetric water content, for the 21 stations over Alaska (Table 3). We assume the available climate measurements are reliable, and the uncertainty comes from other inputs or parameters. The stations have climate observations (21 sites), CALM ALT measurements at 19 sites, and T_{ps} measurements at 12 sites. Climate inputs are listed in Table 3, which are derived from the dataset compiled by Wang et al. (2018). Furthermore, we evaluate the uncertainties of the spatial simulation over entire Alaska and compare with measurements from 53 ALT sites and 117 T_{ps} sites.

For the sensitivity analysis over Alaska, we use a probability distribution of the climate inputs and soil thermal parameters that captures the characteristics of these parameters (Fig. 3). We do not have precise information about vegetation heights and vegetation thermal diffusivities. Thus, we also assume vegetation parameters can be described by a uniform distribution within possible ranges (Table 1). This means that for our sensitivity testing we oversimplify, and climate inputs and vegetation parameters are assumed to be independent of each other.

In the model without parameterization (i.e., Ku-Flex), the inputs and parameters are independent with each other. When we use soil and snow parameterization methods, a few parameters are depending, including soil latent heat, thermal conductivities (thaw and frozen), heat capacities (thaw and frozen), because they are all related to soil water content. However, parsing the interactions among all dependent variables is difficult for the sensitivity analysis based on Monte Carlo method.

2.7. Statistical methods and evaluation metrics

To obtain the statistical characteristics of input parameters from available gridded databases (Fig. 3), we tested 89 probability distribution functions (including Beta, Weibull, Gamma, etc.) provided in the

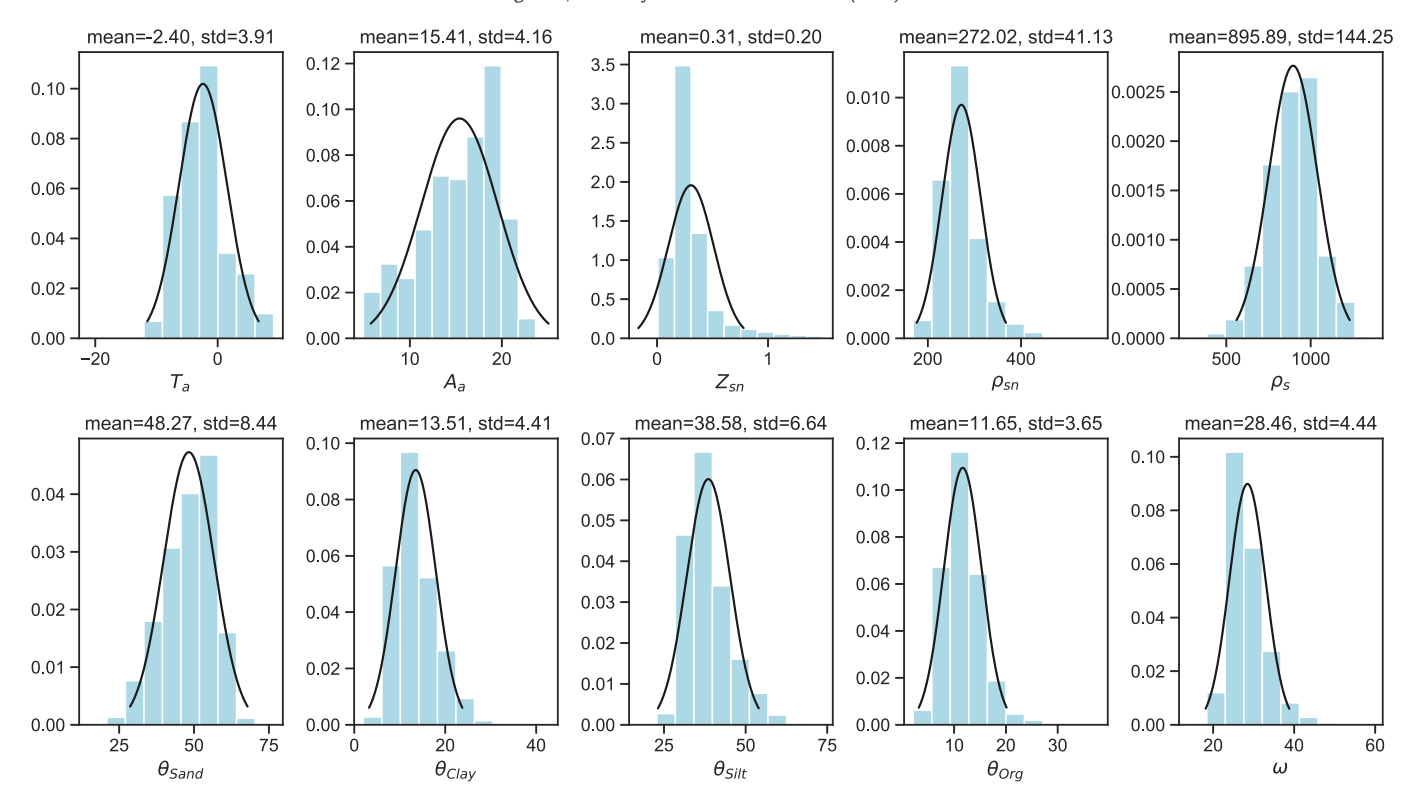


Fig. 3. Histograms of climate inputs and soil thermal parameters. The estimated parameters are shown on the top of each panel.

SciPy python statistics package and calculated the absolute errors. The normal distribution was selected as the optimal form. The Monte Carlo sampling process uses a Latin hypercube sampling (LHS) approach (n=20,000), which is a statistical method to generate a nearrandom sample of parameter values from a multidimensional distribution.

Sensitivity of each parameter is measured by the Pearson correlation coefficient between the input parameter and predicted variables (permafrost temperature, active layer thickness, ground surface temperature, and annual amplitude, see Fig. 4). For a relatively large sample in a parameter study (n > 1000), the critical value of Pearson correlation is about $\pm 0.05 - \pm 0.06$ at 95% confidence level (Cook and Wheater, 2005), i.e., Pearson correlation >0.05 or <-0.05 is statistically significant. In fact, the critical value would be as low as $\sim \pm 0.02$ when n = 20,000 as in our simulations.

We used root-mean-square-error (RMSE) as a performance metric to compare the predicted permafrost temperature and active layer thickness with corresponding in-situ measurements. We calculated standard deviations from all simulation experiments using random parameter combinations to construct error bars (i.e. Figs. 6 and 7).

3. Results

3.1. Sensitivity analysis of Ku model without parameterizations

The Ku model poses that the main controls of permafrost surface temperature T_{ps} are mean annual air temperature T_a , annual amplitude of air temperature A_a , and winter-averaged snow depth Z_{sn} (Fig. 4A). The strongest control on permafrost temperature at the base of the active layer T_{ps} is mean annual air temperature T_a , on average, the correlation between T_{gs} and T_a is 0.80. A_a is another important factor, which has a negative correlation of 0.32 with T_{gs} . Snow depth is ranked as the third most important factor and has a positive correlation of 0.23 with T_{gs} , so that a thickening snowpack implies a warmer permafrost temperature. Thermal conductivity of snow T_{sn} has a considerable effect on T_{ps} . Other parameters show only weak correlation with permafrost surface

temperature T_{ps} . Snow density ρ_{sn} does not appear to directly correlate strongly with T_{ps} , but that might be an underestimation, because snow thermal conductivity is mainly determined by snow density.

The controls of active layer thickness ALT are mean annual air temperature T_a , annual amplitude of air temperature A_a , latent heat of icewater fusion Q_L , and soil thermal conductivity in thawed state K_f (Fig. 4A). Influences from air temperature (T_a and A_a) and snow cover propagate to ALT through permafrost surface temperature, mean annual ground surface temperature, and annual amplitude of ground surface temperature (Eqs. (11)–(13)). As expected, latent heat during phase changes (Q_L) will affect ALT significantly. ALT is positively, but less pronouncedly than permafrost temperature, related to mean annual air temperature (correlation of 0.46). The effect of snow on modeled ALT is limited, but there are distinct differences from snowpack effect on permafrost temperature. The correlation between snow cover and ALT is weak, but negative, which is because this outcome is dominated by localities of warm permafrost and a thick snow cover. For those cases the subsurface stays relatively warm during winter. As an example of such a case, wherein T_{gs} may be close to the freezing point and A_{gs} is very small and Z_{sn} is high (e.g. >1.0 m), the active layer is predicted to be shallow. A real-world example of this effect is at Gakona, AK, where the annual amplitude of soil temperature is only ~5 °C, permafrost temperature is around -0.5 °C, while ALT is ~0.6 m.

3.2. Sensitivity analysis of Ku model with typical snow and soil thermal parameterizations

Under typical snow and soil thermal parameterizations, results show that the main controls of permafrost surface temperature T_{ps} are mean annual air temperature T_a , annual amplitude of air temperature A_a , and winter-averaged snow depth Z_{sn} (Fig. 4B), which is relatively similar to the pattern in Fig. 4A. For the parametrized simulations, the correlations with air temperature weaken slightly, whereas the correlation with snow cover strengthens. However, for ALT simulation, soil water content becomes the most important controlling factor, mainly because the soil thermal properties, including thermal conductivity,

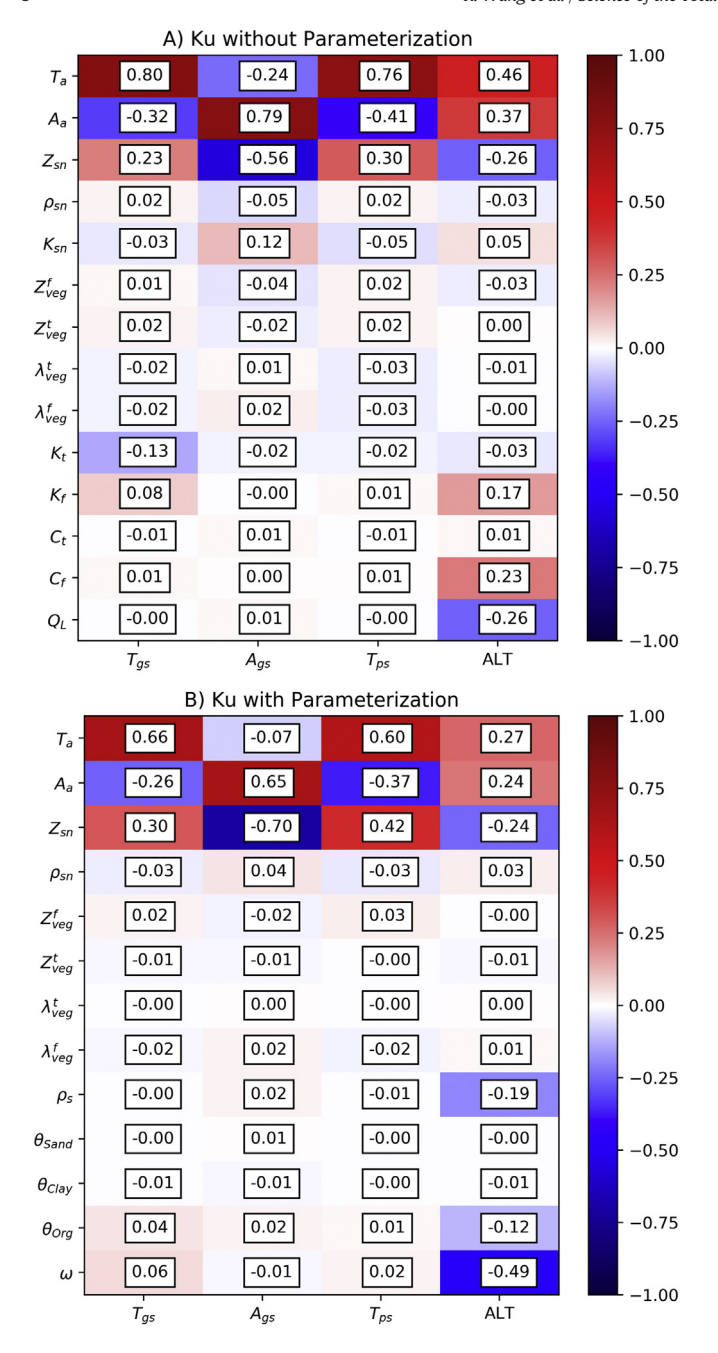


Fig. 4. (A) Pearson correlation coefficients of sensitivity analysis of Ku model without parameterization. (B) Pearson correlation coefficients of sensitivity analysis of Ku model with parameterization. Variable names are listed in Table 1.

heat capacity, and latent heat of phase changes are all connected to soil water content (Eqs. (16)–(20)). Air temperature (T_a and T_a), snow depth (T_a), soil bulk density (T_a), and organic content (T_a) have considerable impact, although relatively smaller than the influence of soil water content.

3.3. Uncertainty evaluation for permafrost simulation over Alaska

By using observed mean annual air temperature T_a , annual amplitude of air temperature A_a , winter-averaged snow depth Z_{sn} , and volumetric soil water content ω , we predict T_{ps} and ALT across 21 permafrost monitoring stations. Simulated permafrost surface temperature T_{ps} is well captured. T_{ps} from GTN-P ranges from -10 to $1.2\,^{\circ}$ C,

which is similar with the predicted permafrost surface temperature. The RMSE between simulated and measured T_{ps} is ~1.0 °C. Comparing measured ALT from the CALM database and T_{ps} from the GTN-P database with the simulations, the overall results indicate a good agreement (Fig. 5A), as had been found in previous studies (Anisimov et al., 1997; Shiklomanov and Nelson, 1999; Streletskiy et al., 2012). The ALT predicted by the Ku model is in a similar range as the CALM measurements across the stations (Table 3), ranging from about 0.3 to 0.7 m. Note that, Bonanza Creek, a site in Interior Alaska, burned in 2011, thus the measured ALTs after that event were excluded in this study. The maximum bias between predicted and observed ALT is at Koluktak, where is a very sandy site with a very thick active layer (~1.2 m), thus the relative bias is not too large (~13%). Overall, RMSE between simulated and measured ALT is ~0.08 m across these stations, ranging from 0.01 to 0.15 m.

Elaborate discussion of different types of permafrost models was presented by Riseborough et al. (2008). Several previous studies compared model predictions with in-situ measurements of ALT in Alaska. Tao et al. (2019) used NASA Catchment Land Surface Model (CLSM) to simulate ALT and showed an error (RMSE) of 0.17 m. Guo et al. (2017) used different climate forcing to drive the Community Land Model, version 4.5 (CLM4.5) model and found errors to range between 0.52 and 0.89 m. Another land surface model, JULES, also produced ALT with a relatively large error (RMSE) (Dankers et al., 2011). The recently calibrated GIPL2 model provided a similar accuracy as this study (Fig. 5A and B) with ALT RMSE of 0.08 m and simulated permafrost temperature an RMSE of 0.7 °C (Jafarov et al., 2012). Note that the sites used in these separate studies were not exactly the same. There are multiple sources of the inter-model differences, including model forcing, structure, and parameterization. Thus, more detailed model intercomparison would be needed to parse the different error sources.

Considering all other variables and parameters as uncertainty source, the simulation uncertainties of ALT and T_{ps} are $\pm 0.02 - \pm 0.10$ m and $\pm 0.20 - \pm 0.38$ °C (Fig. 6). This implies that if T_a , A_a , Z_{sn} , and ω are well known, uncertainty of predictive T_{ps} is small (~0.4 °C). Although uncertainty of predicted ALT (error bars in Fig. 6) is much larger than that of T_{ps} , the uncertainty is generally <0.10 m. Improvements made in other variables or parameters (besides T_a , A_a , Z_{sn} , and ω) may not improve the simulations significantly, which is consistent with the results shown in Fig. 4.

By using air temperature, snow cover, and soil water content from gridded datasets, the bias in both ALT and T_{ps} becomes rather larger, particularly in ALT (Fig. 5C and D). RMSEs of ALT and T_{ps} are 0.26 m and 1.61 °C, respectively. To evaluate the importance of each input, we replace the input here by in-situ measurements in Table 3. Replacing T_a with the data in Table 3, simulated ALT and T_{ps} do not improve significantly. Similarly, replacing A_a will improve slightly simulation of ALT (RMSE reduces to 0.05 m) while T_{ps} doesn't be improved significantly (~0.10 °C). Replacing Z_{sn} will improve significantly the simulations of T_{ps} (RMSE reduces 0.61 °C) while ALT doesn't be improved. Finally, replacing ω will reduce RMSE of ALT ~0.10 m. Therefore, according to these stations data, uncertainty from soil water content might be the most important source in the simulation of ALT and roughly contributes ~40% (0.10 m/0.25 m) of the total uncertainty of simulated ALT when we use gridded data as inputs.

For entire Alaska, we apply the above described, state-of-the-art gridded datasets, including the air temperature and precipitation from SNAP datasets and soil properties from SoilGrids-1km to force our Ku model. Then all available ALT and T_{ps} (not only those data in Table 3) sites are used for validation across entire Alaska. To better comparison, we use the long-term mean of climate inputs during 1996–2015 that is similar to the comprehensive data in Table 3. Expectable, the base running has a larger bias (not shown) similar to what we show in Fig. 5 above.

Comparing with in-situ observations in Table 3, the bias of T_a , A_a , Z_{sn} , and ω from the gridded datasets are about 0.66 °C, 1.38 °C, 0.07 m, and 0.12 m³ m⁻³, indicating A_a and ω might be important uncertainty

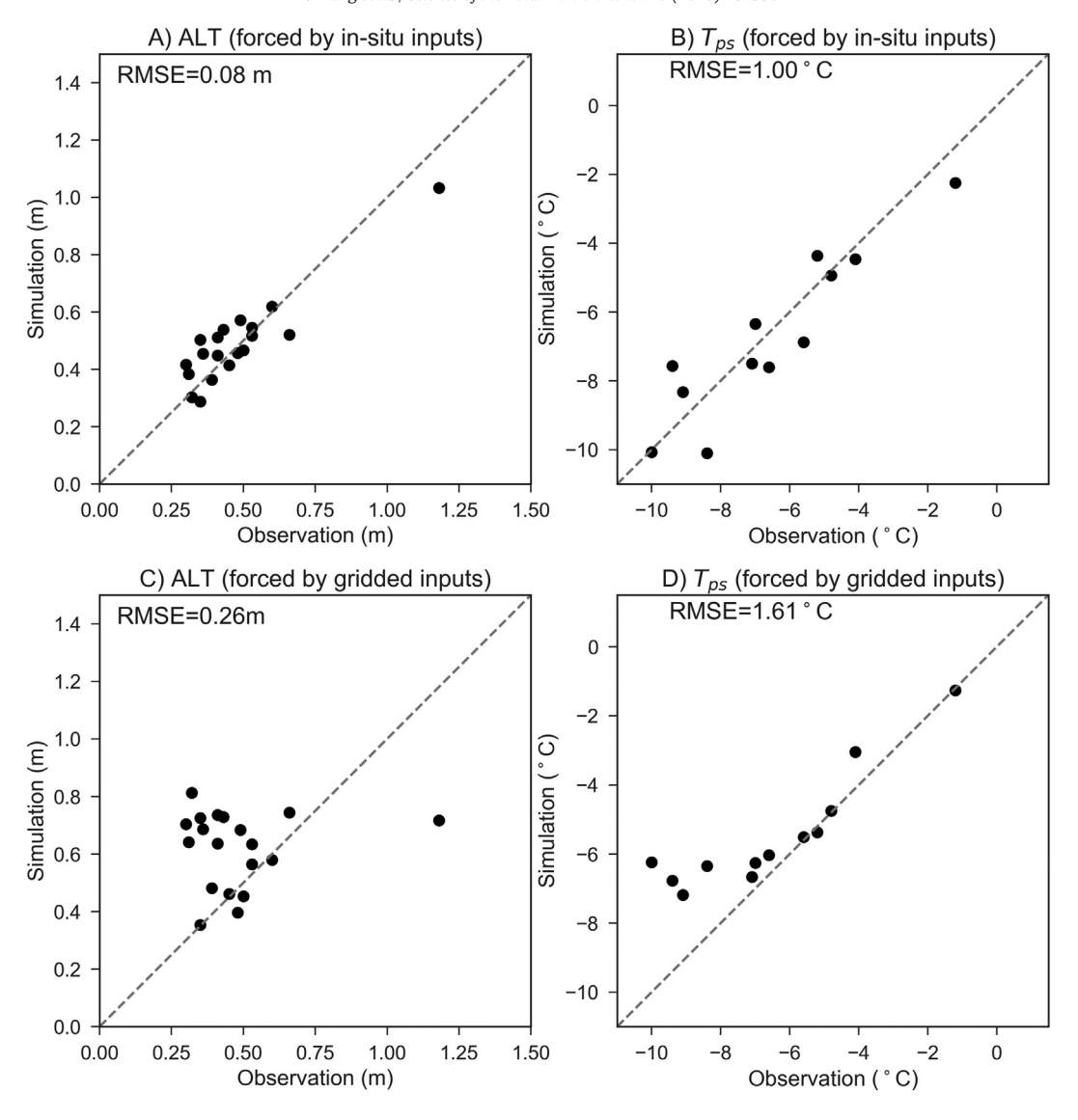


Fig. 5. Validation of simulated ALT (A) and T_{ps} (B) by using climate forcing data listed in Table 1. Validation of simulated ALT (C) and T_{ps} (D) by using the data extracted from SNAP downscaling climate data.

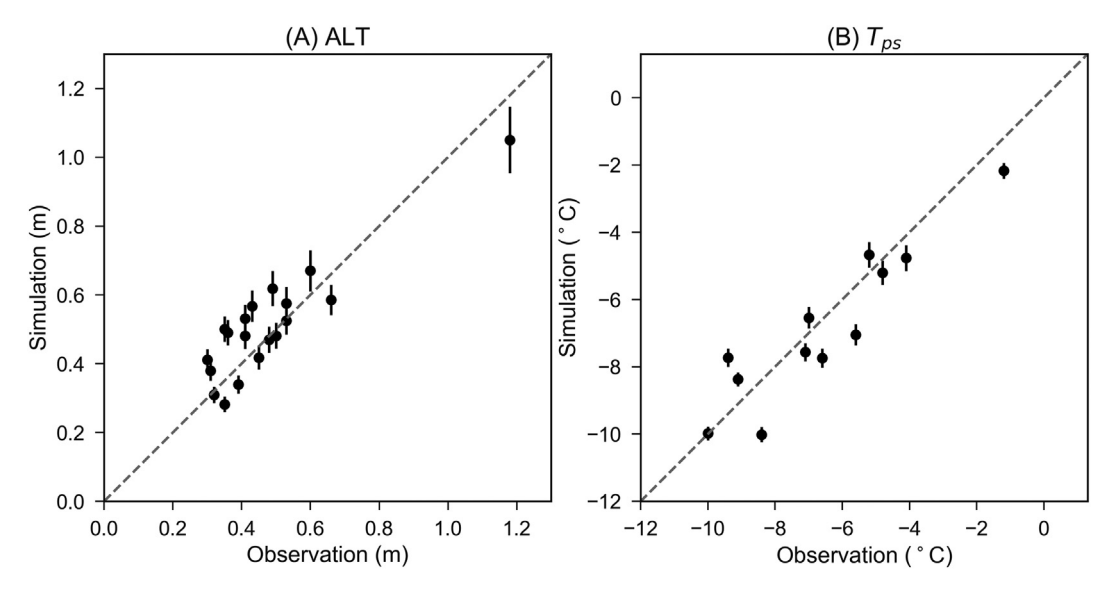


Fig. 6. Uncertainty evaluation of Ku simulations over the stations in Table 3. The available variables in Table 3 are maintained as constants. The unknown parameters are fulfilling with normal distributions shown in Fig. 3.

sources. Using in-situ measurements and corresponding gridded values, we find a linear relationship between gridded (A_a and ω) and in-situ data:

$$Adj_{-}A_{a} = 0.568A_{a} + 7.12$$

 $Adj_{-}\omega = -0.302\omega + 0.490$

where Adj_A_a and Adj_ω are adjusted A_a and ω from the gridded datasets. When we use this relationship to correct bias between gridded and in-situ data, the simulated ALT improves significantly (RMSE reduces from 0.41 m to 0.21 m). As expected, the largest bias is again found at Koluktak. Similar to what we showed before (Fig. 4), T_{ps} does not respond significantly to these adjustments.

As comparisons above show, air temperature and snow depth show a small bias. Assuming air temperature and snow depth are well known, how large would be the uncertainty of Ku model simulations? We evaluate uncertainties from all variables except air temperature and snow depth in ALT and T_{ps} simulations. Simulated ALT can appear quite unreasonable (Fig. 7A), with uncertainty (error bars in Fig. 7A) as much as ~0.6 m or more. When we apply an adjusted ω , simulated ALT improves significantly (Fig. 7C). Uncertainty of simulated ALT reduces to 0.15 \pm 0.04 m (Fig. 7C). Simulated T_{ps} captures the features over these sites (Fig. 7B) and the uncertainty of T_{ps} is generally <0.6 °C (0.56 \pm

0.17 °C, error bars in Fig. 7B). Adjustments of ω are not effectively changing T_{ps} . In other words, once air temperature and snow depth are well constrained, the simulated T_{ps} agrees well with in-situ observations.

4. Discussion

Air temperature is the most important control on Kudryavtsev model predictions of the annual permafrost table temperature. Fortunately, there is an appropriate quality monthly air temperature dataset for Alaska, at a relatively high spatial resolution. Interestingly, the comparison of in-situ and gridded data shows that the gridded reanalysis temperature data is generally higher than in-situ mean annual air temperature (MAAT) (RMSE < 1 °C) (Wang et al., 2018), so this would cause systematic overestimation of permafrost temperature. Some of this overestimation is compensated by a smaller annual temperature amplitude in the reanalysis data as compared to direct observations. Thus, the lower amplitude counteracts the shift in simulated ALT caused by higher MAAT, and the resulting predictions agree well with in-situ observations. For global scale modeling, the bias of gridded air temperature may still cause a significant uncertainty. Anisimov et al. (1997) investigated the uncertainties from gridded air temperature on permafrost model output. Their study showed that four specific datasets, CRU,

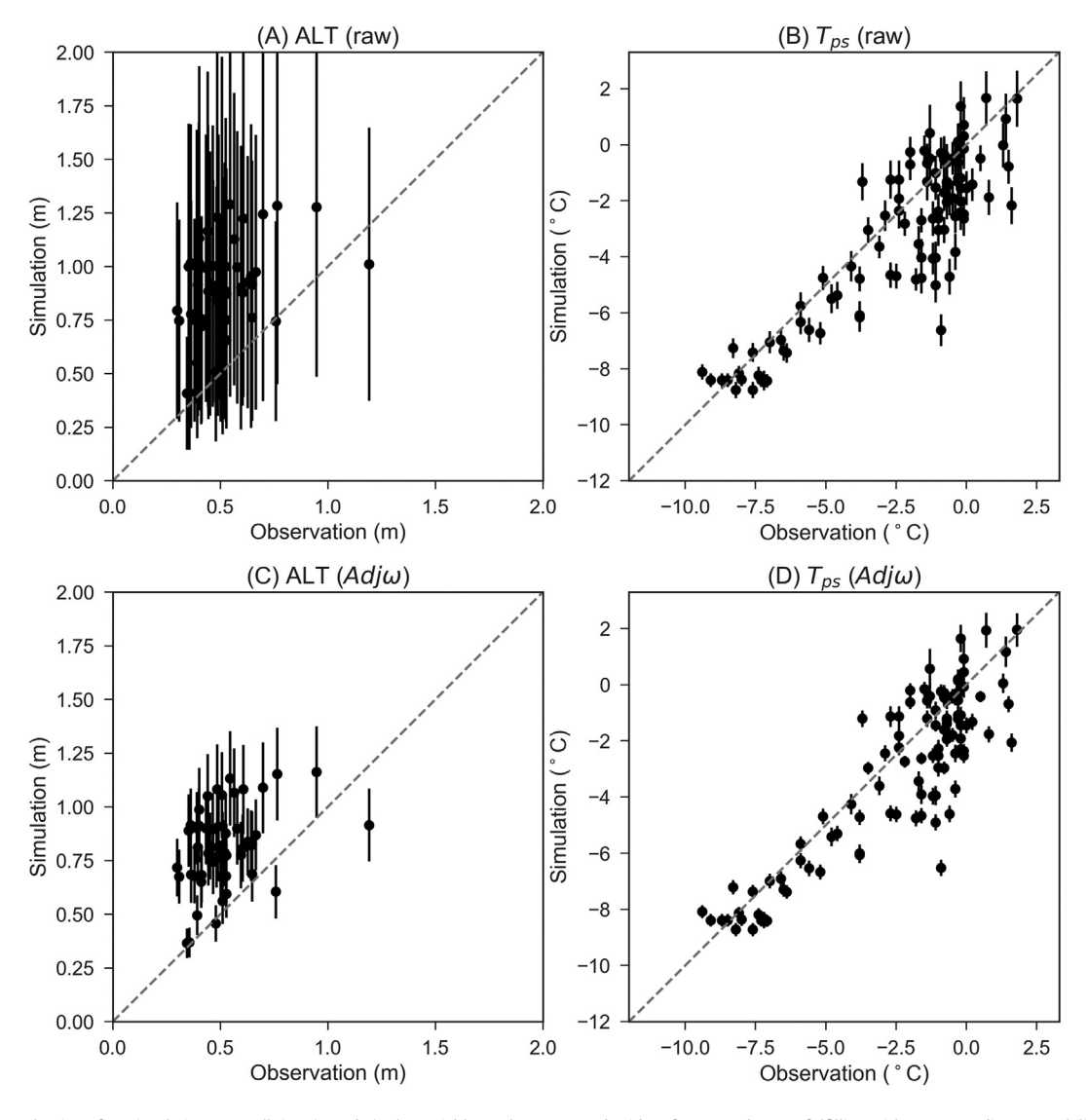


Fig. 7. Uncertainty evaluation of Ku simulations over all sites (A and B). The variables and parameters besides of T_a , A_a , and Z_{sn} are fulfilling with corresponding normal distributions shown in Fig. 3. (C and D) are same with (A and B) but for adjusted ω simulations.

NCEP, ERA, and Willmott & Matsuura, have a departure of $1-2\,^{\circ}\mathrm{C}$ from observations at 455 Russian meteorological stations. That level of uncertainty then affects the estimates of permafrost occurrence and ALT. Notably, the greatest influence is near the southern boundary of permafrost region.

Based on the site-specific results, soil water content is the most sensitive factor in the Ku model beyond more readily available air temperature and snow parameters. Soil moisture influences the simulated ALT in multiple ways, including alteration of soil thermal conductivity, soil bulk density, and heat capacity. This fundamentally is caused by a large component of latent heat during the phase change between ice and water. Our findings imply that we need more accurate water content data as an input to improve predictions of ALT. However, high spatial variability of soil water content provides a significant source of bias, and this parameter may cause large uncertainty when the model is applied for regional scales. From our in-situ data, we find the existing soil moisture data from the SoilGrid 1 km are unable to describe local spatial variations. Soil Moisture Active Passive (SMAP) data (Entekhabi et al., 2010) offers more direct observations than SoilGrid (Colliander et al., 2017; Ma et al., 2017). But one important shortcoming is that SMAP is a relatively new product with data collection started in 2015, which does not allow historical reconstruction. Yet another added complexity is that volumetric water content affects thermal conductivity and heat capacity both in frozen and thaw states. The SMAP data appears to underestimate soil moisture in comparison with ground measurements, especially in cold regions (Ma et al., 2017).

We examined the uncertainties of snow density and snow depth in the model and show in theory, snow density has a limited effect on ALT model predictions. This implies we can assume a constant snow density without introducing a significant bias (assuming snow depth is accurately set as a model input). Unfortunately, snow depth is always derived from snow water equivalent, and thus it depends on (potentially) variable snow density (Zhong et al., 2014). This entanglement of the two parameters introduces a significant bias on estimates of snow depth, and thus using constant snow density would still introduce a bias to permafrost temperature and active layer thickness predictions. The Ku permafrost model requires only a "winter-averaged" snow thickness and density, which may be captured adequately by a simple empirical algorithm (Nelson and Outcalt, 1987; Anisimov et al., 1997). But now that high resolution topography and snow thickness datasets are becoming commonplace, it should be noted that those previous studies mainly considered a relatively coarse spatial resolution, which might conceal local issues in complex topographic regions (Brown et al., 2018).

The effect of the vegetation on soil temperatures were well documented in the classical permafrost studies (e.g. Ershov (1971); Kudryavtsev et al. (1977); Williams and Smith (1989); Yershov and Williams (2004); Harris et al. (2018)). More recent studies indicate the effect of vegetation on permafrost temperatures even in tundra environment (Sturm et al., 2005; Jafarov et al., 2013; Jafarov et al., 2018). Better vegetation parametrization and mapping would thus be necessary to improve the accuracy of permafrost modeling. On the other hand, the Ku model considers only heat transfer processes while the impacts of high vegetation are also related to surface energy balance. In the future, coupling a surface energy balance module would be necessary for solving this issue.

Apart from climatic conditions, soil properties need to be better resolved. For permafrost simulations, thermal conductivity is a controlling factor. Here, we used a simple parameterization approach (Section 2.4). There are many other different methods that require various inputs (Farouki, 1981) that could still be evaluated in more detail. Our analysis also indicated that the peat (organic) layer on near-surface soil is an important buffering layer, which is similar to previous studies (Harp et al., 2016; Jafarov and Schaefer, 2016). It is possible to consider the peat layer in a one dimensional local model (Streletskiy et al., 2012) but a distributed map of thickness of peat at regional scale is currently lacking.

5. Summary

Permafrost models were classified into three main categories by Riseborough et al. (2008): empirical, equilibrium and numerical models. Empirical models relate permafrost occurrence to climate and topographical factors and use empirically derived parameters to determine the response of the active layer and permafrost to these forcings, e.g. as soil properties, moisture conditions and vegetation (key examples are: Nelson et al. (1997); Shiklomanov and Nelson (2002); Zhang (2005); Shiklomanov et al. (2010)). The other end-member are numerical models that are used to solve freeze-thaw problems over a short time scale, where the transient effects of phase change are important (Williams and Smith, 1989), i.e. in engineering applications. These transient numerical models (e.g., Ling and Zhang (2004); Westermann et al. (2013); Westermann et al. (2016); Nicolsky et al. (2017)) have a higher computational requirements, while being more accurate in determination of the temperature field and phase change boundary dynamics.

In this study, we use a model that falls in the intermediate category, those models classified as equilibrium models. Typically, these equilibrium models use transfer functions between the air and ground temperatures to define the active layer depth. The Kudryavtsev Model, N-factor, TTOP, and GIPL 1.0 models are all classified as equilibrium models (Kudryavtsev et al. (1977); Romanovsky and Osterkamp (1995); Nelson et al. (1997); Romanovsky and Osterkamp (1997); Sazonova and Romanovsky (2003); Gisnås et al. (2013)). These models are appropriate in situations where data is sparse, such as vast spatial scales, or for simulating long time scales – e.g. permafrost landscape dynamics over glacial cycles.

Here, we investigated the sensitivity of the Kudryavtsev's active layer model by Monte Carlo simulations and compared predictions with a comprehensive dataset of in-situ ground surface temperature and active layer thickness observations over the entire Alaskan region.

We find that predicted permafrost surface temperature is dominantly controlled by 1) mean annual air temperature, 2) annual temperature amplitude, and 3) winter-averaged snow thickness. Uncertainty of predicted permafrost temperature is relatively small, when air temperature and snow depth are well constrained. Active layer thickness can be predicted with uncertainty of ~0.08 m. However, under given air temperature and snow conditions, soil water content bias can significantly alter modeled active layer thickness (up to 40% error). In other words, if soil water content has a large bias, any improvements in other parameters may not significantly improve the active layer predictions of the Kudryavtsev's model. Ultimately, many inputs and parameters are interdependent in the real world. For example, air temperature is closely related to snow cover. Thus, parsing the interactions among dependent variables would to be an important task in the future.

We designed Ku model to be a part of the permafrost toolbox (Overeem et al., 2018), and for this reason it includes a Python basic model interface, that allows information to be passed easily between it and other compatible models. More challenging problems in permafrost processes involve assembling models that couple the Ku model as a component with other Earth surface process models. We envision Ku model to be applied to explore feedbacks between long-term geomorphic processes. Such coupled processes are still largely unexplored, but they have been shown to be potentially significant in topographically complex terrain (Bovy et al., 2016; Shelef et al., 2017).

CRediT authorship contribution statement

K. Wang: Conceptualization, Formal analysis, Methodology, Software, Visualization, Writing - original draft, Writing- Reviewing and Editing. **E. Jafarov:** Conceptualization, Formal analysis, Methodology, Software, Writing- Reviewing and Editing. **I. Overeem:** Conceptualization, Formal analysis, Methodology, Software, Visualization, Writing-Reviewing and Editing.

Declaration of competing interest

The authors declare that there are no conflicts of interest.

Acknowledgements

This study was supported by the US National Science Foundation (Awards nos: 1503559 and 1831623), the National Natural Science Foundation of China (Award no: 41701064), and the Next-Generation Ecosystem Experiments Arctic (NGEE-Arctic) Project, Department of Energy Office of Science. The codes of the Ku model and sensitivity analysis are available at the GitHub repository of the Permafrost Modeling Toolbox (https://github.com/permamodel/permamodel/releases). We would like to thank Dr. Ross Brown (Environment and Climate Change Canada) for providing support for their snow model and calculations. SNAP datasets are available at http://data.snap.uaf.edu/data/Base/AK_CAN_2km/historical/CRU_TS/. SoilGrids-1km datasets are available at https://files.isric.org/soilgrids/data/aggregated/1km/. Color Alaska Shaded Relief – 200-Meter Resolution, Albers projection is available at https://www.sciencebase.gov/catalog/item/

4f4e4a85e4b07f02db64d5cb. A snow classification map [ftp://gliston.cira.colostate.edu/snow_classification/] and land cover map [https://www.earthenv.org/landcover] are used for driving the simple snow accumulative model. Numerical simulations were performed on the Community Surface Dynamics Modeling System (CSDMS) High Performance Computing Cluster, supported and maintained by the research computing center of University of Colorado Boulder. We appreciate the editors, Dr. Christian Herrera and Dr. Paulo Pereira, and two reviewers for their thoughtful comments towards improving our manuscript.

References

- Anisimov, O.A., Shiklomanov, N.I., Nelson, F.E., 1997. Global warming and active-layer thickness: results from transient general circulation models. Glob. Planet. Chang. 15, 61–77. https://doi.org/10.1016/S0921-8181(97)00009-X.
- Bieniek, P.A., Bhatt, U.S., Thoman, R.L., Angeloff, H., Partain, J., Papineau, J., Fritsch, F., Holloway, E., Walsh, J.E., Daly, C., Shulski, M., Hufford, G., Hill, D.F., Calos, S., Gens, R., 2012. Climate divisions for Alaska based on objective methods. J. Appl. Meteorol. Climatol. 51, 1276–1289. https://doi.org/10.1175/JAMC-D-11-0168.1.
- Bieniek, P.A., Walsh, J.E., Thoman, R.L., Bhatt, U.S., 2014. Using climate divisions to analyze variations and trends in Alaska temperature and precipitation. J. Clim. 27, 2800–2818. https://doi.org/10.1175/JCLI-D-13-00342.1.
- Biskaborn, B.K., Lanckman, J.P., Lantuit, H., Elger, K., Streletskiy, D.A., Cable, W.L., Romanovsky, V.E., 2015. The new database of the Global Terrestrial Network for Permafrost (GTN-P). Earth System Science Data 7, 245–259. https://doi.org/10.5194/ essd-7-245-2015.
- Bovy, B., Braun, J., Demoulin, A., 2016. A new numerical framework for simulating the control of weather and climate on the evolution of soil-mantled hillslopes. Geomorphology 263, 99–112. https://doi.org/10.1016/j.geomorph.2016.03.016.
- Brown, J., Hinkel, K.M., Nelson, F.E., 2000. The circumpolar active layer monitoring (CALM) program: research designs and initial results. Polar Geogr. 24, 166–258. https://doi.org/10.1080/10889370009377698.
- Brown, R.D., Brasnett, B., Robinson, D., 2003. Gridded North American monthly snow depth and snow water equivalent for GCM evaluation. Atmosphere-Ocean 41, 1–14. https://doi.org/10.3137/ao.410101.
- Brown, R., Tapsoba, D., Derksen, C., 2018. Evaluation of snow water equivalent datasets over the Saint-Maurice river basin region of southern Québec. Hydrol. Process. 32, 2748–2764. https://doi.org/10.1002/hyp.13221.
- Burgess, M.M., Smith, S.L., Brown, J., Romanovsky, V., Hinkel, K., 2000. Global Terrestrial Network for Permafrost (GTNet-P): permafrost monitoring contributing to global climate observations. Geological Survey of Canada, Current Research 1–8.
- Colliander, A., Jackson, T.J., Bindlish, R., Chan, S., Das, N., Kim, S.B., Cosh, M.H., Dunbar, R.S., Dang, L., Pashaian, L., Asanuma, J., Aida, K., Berg, A., Rowlandson, T., Bosch, D., Caldwell, T., Caylor, K., Goodrich, D., al Jassar, H., Lopez-Baeza, E., Martínez-Fernández, J., González-Zamora, A., Livingston, S., McNairn, H., Pacheco, A., Moghaddam, M., Montzka, C., Notarnicola, C., Niedrist, G., Pellarin, T., Prueger, J., Pulliainen, J., Rautiainen, K., Ramos, J., Seyfried, M., Starks, P., Su, Z., Zeng, Y., van der Velde, R., Thibeault, M., Dorigo, W., Vreugdenhil, M., Walker, J.P., Wu, X., Monerris, A., O'Neill, P.E., Entekhabi, D., Njoku, E.G., Yueh, S., 2017. Validation of SMAP surface soil moisture products with core validation sites. Remote Sens. Environ. 191, 215–231. https://doi.org/10.1016/j.rse.2017.01.021.
- Cook, P.A., Wheater, P., 2005. Using Statistics to Understand the Environment. Routledge, London, UK.
- Dankers, R., Burke, E.J., Price, J., 2011. Simulation of permafrost and seasonal thaw depth in the JULES land surface scheme. Cryosphere 5, 773–790. https://doi.org/10.5194/tc-5-773-2011.

- Entekhabi, D., Njoku, E.G., O'Neill, P.E., Kellogg, K.H., Crow, W.T., Edelstein, W.N., Entin, J.K., Goodman, S.D., Jackson, T.J., Johnson, J., Kimball, J., Piepmeier, J.R., Koster, R.D., Martin, N., McDonald, K.C., Moghaddam, M., Moran, S., Reichle, R., Shi, J.C., Spencer, M.W., Thurman, S.W., Tsang, L., Zyl, J.V., 2010. The Soil Moisture Active Passive (SMAP) mission. Proceedings of the IEEE. 98, pp. 704–716.
- Ershov, E.D., 1971. Approximate quantitative estimate of the influence of various factors of the natural situation on the temperature regime of rocks. Merzlotnyye issledovaniya. 1. Moscow State University.
- Farouki, O.T., 1981. Thermal Properties of Soils. Cold Regions Research and Engineering
 Lab. Hanover. NH.
- Gisnås, K., Etzelmüller, B., Farbrot, H., Schuler, T.V., Westermann, S., 2013. CryoGRID 1.0: permafrost distribution in Norway estimated by a spatial numerical model. Permafr. Periglac. Process. 24, 2–19. https://doi.org/10.1002/ppp.1765.
- Goodrich, L.E., 1982. The influence of snow cover on the ground thermal regime. Can. Geotech. J. 19, 421–432. https://doi.org/10.1139/t82-047.
- Guo, D., Wang, H., Wang, A., 2017. Sensitivity of historical simulation of the permafrost to different atmospheric forcing data sets from 1979 to 2009. J. Geophys. Res. Atmos. 122, 12,269–12,284. https://doi.org/10.1002/2017JD027477.
- Harp, D.R., Atchley, A.L., Painter, S.L., Coon, E.T., Wilson, C.J., Romanovsky, V.E., Rowland, J.C., 2016. Effect of soil property uncertainties on permafrost thaw projections: a calibration-constrained analysis. Cryosphere 10, 341–358. https://doi.org/10.5194/tc-10-341-2016.
- Harris, S.A., Brouchkov, A., Guodong, C., 2018. Geocryology: Characteristics and Use of Frozen Ground and Permafrost Landforms. CRC Press, London, UK.
- Hengl, T., de Jesus, J.M., MacMillan, R.A., Batjes, N.H., Heuvelink, G.B.M., Ribeiro, E., Samuel-Rosa, A., Kempen, B., Leenaars, J.G.B., Walsh, M.G., Gonzalez, M.R., 2014. SoilGrids1km — global soil information based on automated mapping. PLoS ONE 9, e105992. https://doi.org/10.1371/journal.pone.0105992.
- Hijmans, R.J., Cameron, S.E., Parra, J.L., Jones, P.G., Jarvis, A., 2005. Very high resolution interpolated climate surfaces for global land areas. Int. J. Climatol. 25, 1965–1978. https://doi.org/10.1002/joc.1276.
- Hugelius, G., Tarnocai, C., Broll, G., Canadell, J.G., Kuhry, P., Swanson, D.K., 2013. The Northern Circumpolar Soil Carbon Database: spatially distributed datasets of soil coverage and soil carbon storage in the northern permafrost regions. Earth System Science Data 5, 3–13. https://doi.org/10.5194/essd-5-3-2013.
- Jafarov, E., Schaefer, K., 2016. The importance of a surface organic layer in simulating permafrost thermal and carbon dynamics. Cryosphere 10, 465–475. https://doi.org/10.5194/tc-10-465-2016.
- Jafarov, E.E., Marchenko, S.S., Romanovsky, V.E., 2012. Numerical modeling of permafrost dynamics in Alaska using a high spatial resolution dataset. Cryosphere 6, 613–624. https://doi.org/10.5194/tc-6-613-2012.
- Jafarov, E.E., Romanovsky, V.E., Genet, H., McGuire, A.D., Marchenko, S.S., 2013. The effects of fire on the thermal stability of permafrost in lowland and upland black spruce forests of interior Alaska in a changing climate. Environ. Res. Lett. 8, 35030. https://doi. org/10.1088/1748-9326/8/3/035030.
- Jafarov, E.E., Coon, E.T., Harp, D.R., Wilson, C.J., Painter, S.L., Atchley, A.L., Romanovsky, V.E., 2018. Modeling the role of preferential snow accumulation in through talik development and hillslope groundwater flow in a transitional permafrost landscape. Environ. Res. Lett. 13, 105006. https://doi.org/10.1088/1748-9326/aadd30.
- Jorgenson, M.T., Kenji, Y., Mikhail, K., Shur, Y., 2008. Permafrost characteristics of Alaska. Proceedings of the Ninth International Conference on Permafrost. 29. University of Alaska, pp. 121–122.
- Koven, C.D., Ringeval, B., Friedlingstein, P., Ciais, P., Cadule, P., Khvorostyanov, D., Krinner, G., Tarnocai, C., 2011. Permafrost carbon-climate feedbacks accelerate global warming. Proc. Natl. Acad. Sci. U. S. A. 108, 14769–14774. https://doi.org/10.1073/pnas.1103910108.
- Kudryavtsev, V.A., Garagulya, L.S., Melamed, V.G., 1977. Fundamentals of Frost Forecasting in Geological Engineering Investigations (Osnovy Merzlotnogo Prognoza pri Inzhenerno-Geologicheskikh Issledovaniyakh). U.S. Army Cold Regions Research and Engineering Laboratory, Hanover, NH.
- Ling, F., Zhang, T., 2004. A numerical model for surface energy balance and thermal regime of the active layer and permafrost containing unfrozen water. Cold Reg. Sci. Technol. 38, 1–15. https://doi.org/10.1016/S0165-232X(03)00057-0.
- Lunardini, V.J., 1981. Heat Transfer in Cold Climates. Van Nostrand Reinhold Company, New York, USA.
- Ma, C., Li, X., Wei, L., Wang, W., 2017. Multi-scale validation of SMAP soil moisture products over cold and arid regions in northwestern China using distributed ground observation data. Remote Sens. 9, 327. https://doi.org/10.3390/rs9040327.
- MacDougall, A.H., 2016. Catalyst for deglaciation. Nat. Geosci. 9, 648–649. https://doi.org/ 10.1038/ngeo2802.
- Marchenko, S., Vladimir, R., Tipenko, G., 2008. Numerical Modeling of Spatial Permafrost Dynamics in Alaska. 29. Institute of Northern Engineering, University of Alaska Fairbanks, pp. 1125–1130.
- McGuire, A.D., Koven, C., Lawrence, D.M., Clein, J.S., Xia, J.Y., Beer, C., Burke, E., Chen, G.S., Chen, X.D., Delire, C., Jafarov, E., MacDougall, A.H., Marchenko, S., Nicolsky, D., Peng, S.S., Rinke, A., Saito, K., Zhang, W.X., Alkama, R., Bohn, T.J., Ciais, P., Decharme, B., Ekici, A., Gouttevin, I., Hajima, T., Hayes, D.J., Ji, D.Y., Krinner, G., Lettenmaier, D.P., Luo, Y.Q., Miller, P.A., Moore, J.C., Romanovsky, V., Schadel, C., Schaefer, K., Schuur, E.A.G., Smith, B., Sueyoshi, T., Zhuang, Q.L., 2016. Variability in the sensitivity among model simulations of permafrost and carbon dynamics in the permafrost region between 1960 and 2009. Glob. Biogeochem. Cycles 30, 1015–1037. https://doi.org/10.1002/2016GB005405.
- McGuire, A.D., Lawrence, D.M., Koven, C., Clein, J.S., Burke, E., Chen, G., Jafarov, E., MacDougall, A.H., Marchenko, S., Nicolsky, D., Peng, S., Rinke, A., Ciais, P., Gouttevin, I., Hayes, D.J., Ji, D., Krinner, G., Moore, J.C., Romanovsky, V., Schadel, C., Schaefer, K., Schuur, E.A.G., Zhuang, Q., 2018. Dependence of the evolution of carbon dynamics

- in the northern permafrost region on the trajectory of climate change. Proc. Natl. Acad. Sci. U. S. A. 115, 3882–3887. https://doi.org/10.1073/pnas.1719903115.
- Melvin, A.M., Larsen, P., Boehlert, B., Neumann, J.E., Chinowsky, P., Espinet, X., Martinich, J., Baumann, M.S., Rennels, L., Bothner, A., Nicolsky, D.J., Marchenko, S.S., 2017. Climate change damages to Alaska public infrastructure and the economics of proactive adaptation. Proc. Natl. Acad. Sci. U. S. A. 114, E122–E131. https://doi.org/10.1073/ ppas 1611056113
- Moon, T.A., Overeem, I., Druckenmiller, M., Holland, M., Huntington, H., Kling, G., Lovecraft, A.L., Miller, G., Scambos, T., Schädel, C., Schuur, E.A.G., Trochim, E., Wiese, F., Williams, D., Wong, G., 2019. The expanding footprint of rapid Arctic change. Earth's Future 7, 212–218. https://doi.org/10.1029/2018EF001088.
- Nelson, F.E., Outcalt, S.I., 1987. A computational method for prediction and regionalization of permafrost. Arct. Alp. Res. 279–288.
- Nelson, F.E., Shiklomanov, N.I., Mueller, G.R., Hinkel, K.M., Walker, D.A., Bockheim, J.G., 1997. Estimating active-layer thickness over a large region: Kuparuk River basin, Alaska. USA. Arct. Alp. Res. 367–378.
- Nicolsky, D.J., Romanovsky, V.E., Panda, S.K., Marchenko, S.S., Muskett, R.R., 2017. Applicability of the ecosystem type approach to model permafrost dynamics across the Alaska North Slope. J. Geophys. Res. Earth Surf. 122, 50–75.
- Nowacki, G., Spencer, P., Brock, T., Fleming, M., Jorgenson, T., 2001. Ecoregions of Alaska and Neighboring Territory (Map). US Geological Survey, Reston, VA.
- Overeem, Irina, Jafarov, Elchin, Wang, Kang, Schaefer, Kevin, Stewart, Scott, Clow, Gary, Piper, Mark, Elshorbany, Yasin, 2018. A modeling toolbox for permafrost landscapes. Eos, Transactions American Geophysical Union (Online), p. 99.
- Panda, S.K., Romanovsky, V.E., Marchenko, S.S., 2016. High-resolution Permafrost Modeling in Arctic National Parks of Alaska. In preparation.
- Peckham, S.D., Hutton, E.W.H., Norris, B., 2013. A component-based approach to integrated modeling in the geosciences: the design of CSDMS. Comput. Geosci. 53, 3–12. https://doi.org/10.1016/j.cageo.2012.04.002.
- Riseborough, D., Shiklomanov, N., Etzelmüller, B., Gruber, S., Marchenko, S., 2008. Recent advances in permafrost modelling. Permafr. Periglac. Process. 19, 137–156. https:// doi.org/10.1002/ppp.615.
- Romanovsky, V.E., Osterkamp, T.E., 1995. Interannual variations of the thermal regime of the active layer and near-surface permafrost in northern Alaska. Permafr. Periglac. Process. 6, 313–335. https://doi.org/10.1002/ppp.3430060404.
- Romanovsky, V.E., Osterkamp, T.E., 1997. Thawing of the active layer on the coastal plain of the Alaskan Arctic. Permafr. Periglac. Process. 8, 1–22. https://doi.org/10.1002/(SICI)1099-1530(199701)8:1<1::AID-PPP243>3.0.CO;2-U.
- Sazonova, T.S., Romanovsky, V.E., 2003. A model for regional-scale estimation of temporal and spatial variability of active layer thickness and mean annual ground temperatures. Permafr. Periglac. Process. 14, 125–139. https://doi.org/10.1002/ppp.449.
- Schuur, E.A., McGuire, A.D., Schadel, C., Grosse, G., Harden, J.W., Hayes, D.J., Hugelius, G., Koven, C.D., Kuhry, P., Lawrence, D.M., Natali, S.M., Olefeldt, D., Romanovsky, V.E., Schaefer, K., Turetsky, M.R., Treat, C.C., Vonk, J.E., 2015. Climate change and the permafrost carbon feedback. Nature 520, 171–179. https://doi.org/10.1038/nature14338
- Shelef, E., Rowland, J.C., Wilson, C.J., Hilley, G.E., Mishra, U., Altmann, G.L., Ping, C.-L., 2017. Large uncertainty in permafrost carbon stocks due to hillslope soil deposits. Geophys. Res. Lett. 44, 6134–6144. https://doi.org/10.1002/2017GL073823.
- Shiklomanov, N.I., Nelson, F.E., 1999. Analytic representation of the active layer thickness field, Kuparuk River Basin, Alaska. Ecol. Model. 123, 105–125. https://doi.org/ 10.1016/S0304-3800(99)00127-1.
- Shiklomanov, N.I., Nelson, F.E., 2002. Active-layer mapping at regional scales: a 13-year spatial time series for the Kuparuk region, north-central Alaska. Permafr. Periglac. Process. 13, 219–230. https://doi.org/10.1002/ppp.425.
- Shiklomanov, N.I., Nelson, F.E., Streletskiy, D.A., Hinkel, K.M., Brown, J., 2008. The circumpolar active layer monitoring (CALM) program: data collection, management, and dissemination strategies. Proceedings of the Ninth International Conference on Permafrost. 29. Institute of Northern Engineering Fairbanks, Alaska.

- Shiklomanov, N.I., Streletskiy, D.A., Nelson, F.E., Hollister, R.D., Romanovsky, V.E., Tweedie, C.E., Bockheim, J.G., Brown, J., 2010. Decadal variations of active-layer thickness in moisture-controlled landscapes, Barrow, Alaska. J. Geophys. Res. Biogeosci. 115, G00l04. https://doi.org/10.1029/2009JG001248.
- Shiklomanov, N., Frederick, N., Dmitry, S., Biskaborn, B.K., 2016. Long-term Active-layer Dynamics: Results of 22 Years of Field Observations in Northern Hemisphere Permafrost Regions. AGU. San Francisco.
- Streletskiy, D.A., Shiklomanov, N.I., Nelson, F.E., 2012. Spatial variability of permafrost active-layer thickness under contemporary and projected climate in Northern Alaska. Polar Geogr. 35, 95–116. https://doi.org/10.1080/1088937X.2012.680204.
- Sturm, M., Holmgren, J., Liston, C.E., 1995. A seasonal snow cover classification system for local to global applications. J. Clim. 8, 1261–1283. https://doi.org/10.1175/1520-0442 (1995)008<1261;ASSCCS>2.0.CO:2.
- Sturm, M., Tom, D., Charles, R., Liston, G.E., 2005. Changing snow and shrub conditions affect albedo with global implications. J. Geophys. Res. Biogeosci. 110, G01004. https://doi.org/10.1029/2005JG000013.
- Tao, J., Koster, R.D., Reichle, R.H., Forman, B.A., Xue, Y., Chen, R.H., Moghaddam, M., 2019. Permafrost variability over the Northern Hemisphere based on the MERRA-2 reanalysis. Cryosphere 13, 2087–2110. https://doi.org/10.5194/tc-13-2087-2019.
- Tarnocai, C., Canadell, J.G., Schuur, E.A.G., Kuhry, P., Mazhitova, G., Zimov, S., 2009. Soil organic carbon pools in the northern circumpolar permafrost region. Glob. Biogeochem. Cycles 23, GB2023. https://doi.org/10.1029/2008GB003327.
- Tuanmu, M.-N., Jetz, W., 2014. A global 1-km consensus land-cover product for biodiversity and ecosystem modelling. Glob. Ecol. Biogeogr. 23, 1031–1045. https://doi.org/ 10.1111/geb.12182.
- Walsh, J.E., Bhatt, U.S., Littell, J.S., Leonawicz, M., Lindgren, M., Kurkowski, T.A., Bieniek, P.A., Thoman, R., Gray, S., Rupp, T.S., 2018. Downscaling of climate model output for Alaskan stakeholders. Environ. Model. Softw. 110, 38–51. https://doi.org/10.1016/j.envsoft.2018.03.021.
- Wang, K., Jafarov, E., Overeem, I., Romanovsky, V., Schaefer, K., Clow, G., Urban, F., Cable, W., Piper, M., Schwalm, C., Zhang, T.J., Kholodov, A., Sousanes, P., Loso, M., Hill, K., 2018. A synthesis dataset of permafrost-affected soil thermal conditions for Alaska, USA. Earth System Science Data 10, 2311–2328. https://doi.org/10.5194/essd-10-2311-2018.
- Westermann, S., Schuler, T.V., Gisnås, K., Etzelmüller, B., 2013. Transient thermal modeling of permafrost conditions in Southern Norway. Cryosphere 7, 719–739. https://doi.org/10.5194/tc-7-719-2013.
- Westermann, S., Østby, T.I., Gisnås, K., Schuler, T.V., Etzelmüller, B., 2015. A ground temperature map of the North Atlantic permafrost region based on remote sensing and reanalysis data. Cryosphere 9, 1303–1319. https://doi.org/10.5194/tc-9-1303-2015.
- Westermann, S., Langer, M., Boike, J., Heikenfeld, M., Peter, M., Etzelmüller, B., Krinner, G., 2016. Simulating the thermal regime and thaw processes of ice-rich permafrost ground with the land-surface model CryoGrid 3. Geosci. Model Dev. 9, 523–546. https://doi.org/10.5194/gmd-9-523-2016.
- Williams, P.J., Smith, M.W., 1989. The Frozen Earth Fundamentals of Geocryology. Cambridge University Press, Cambridge, UK.
- Yershov, E.D., Williams, P.J., 2004. General Geocryology. Cambridge university press.
- Zhang, T., 2005. Influence of the seasonal snow cover on the ground thermal regime: an overview. Rev. Geophys. 43, RG4002. https://doi.org/10.1029/2004RG000157.
- Zhang, T., Osterkamp, T.E., Stamnes, K., 1996. Influence of the depth hoar layer of the seasonal snow cover on the ground thermal regime. Water Resour. Res. 32, 2075–2086. https://doi.org/10.1029/96WR00996.
- Zhang, T., Barry, R.G., Knowles, K., Heginbottom, J.A., Brown, J., 1999. Statistics and characteristics of permafrost and ground-ice distribution in the Northern Hemisphere. Polar Geogr. 23, 132–154. https://doi.org/10.1080/10889370802175895.
- Zhong, X., Zhang, T., Wang, K., 2014. Snow density climatology across the former USSR. Cryosphere 8, 785–799. https://doi.org/10.5194/tc-8-785-2014.